PROGRESS REPORT NAG 5 1838

Ground Truth Spectrometry and Imagery of Eruption Clouds to Maximize Utility of Satellite Imagery

William I. Rose
Phone #: (906) 487-2531
Fax #: (906) 487-3371
E-mail address: raman@mtu.edu
Mailing address: Geological Engineering, Geology and Geophysics, 1400 Townsend Dr., Michigan Technological University, Houghton, MI 49931, USA

ACTIVITIES (January - June 1993):

1. **Experiments with thermal imaging infrared radiometers.** A new AGEMA 900 series radiometer, equipped with an array of filters and calibrated, was purchased by Michigan Tech. Our group did field experiments and designed a laboratory system for controlled study of simulated ash clouds in our laboratory.

2. **Participation in the Federal Aviation Administration Workshop on Old Volcanic Ash Clouds in Washington, D. C.** Presented two papers (see attached).

3. **Development of radiative transfer method to retrieve particle sizes, optical depth, and particle mass burdens in volcanic clouds, using AVHRR thermal infrared bands 4 and 5.** Finished and submitted paper to JGR/Atmospheres, completing one of the proposals principal objectives (see attached).

ACTIVITIES (July - December 1993):

1. **Development of a radiative transfer model to retrieve particle sizes, optical depth and volcanic ash mass burdens in volcanic clouds, using TIMS, MODIS and ASTER.** The new generation of sensors will allow us to apply the same principles to multiple bands of data, allowing better constrained and more robust results.

2. **Participation in American Geophysical Union Fall Meeting.** Presentation of three papers.

RELATED PUBLICATIONS

Hossli, R. J., Rose, W. I. and K. R. Kogler, 1992, Digital processing of TM scenes for mapping of young lavas at Central American volcanoes, AGU Fall Meeting, *EOS* supplement, p. 613.

Rose, W. I. and D. J. Schneider, 1992, Automatic volcanic cloud mapping using AVHRR, AGU Fall Meeting, *EOS* supplement, p. 493.

Rose, W. I., Schneider, D. J., and S. Wen, 1993, Possible use of AVHRR for determining ash burdens in volcanic clouds: preliminary work on Crater Peak/Spurr Data, Federal Aviation Administration Workshop on Old Volcanic Ash Clouds, Washington, D. C., April 22-23.

Rose, W. I., S. Wen and D. J. Schneider, 1993, Satellite based estimates of ash content of drifting volcanic clouds, *EOS supplement,* in press.

Schneider, D. J. and W. I. Rose, 1993, AVHRR observations of the volcanic ash cloud from Pinatubo Volcano, Federal Aviation Administration Workshop on Old Volcanic Ash Clouds, Washington, D. C., April 22-23.

Schneider, D. J. and W. I. Rose, 1992, Comparison of AVHRR and TOMS imagery of volcanic clouds from Pinatubo Volcano, AGU Fall Meeting, San Francisco, CA, December.

Wang, Z., Rose, W. I., and A. Kostinski, 1992, Eruption cloud opacity related to particle mass concentration, size, and wavelength, AGU Fall Meeting, *EOS* supplement, p. 614.

Wen, S. and W. I. Rose, 1993, Retrieval of particle sizes and masses in volcanic clouds using AVHRR bands 4 and 5, *J. Geophys. Res.*, submitted in July.

Digital Processing of TM scenes for mapping of young lavas at Central American volcanoes

Richard J. Hossli, William I. Rose and Kimberly R. Kogler (Geological Engineering, Michigan Technological University, Houghton, MI 49931; 906-487-2531; E-mail: tack@mtu.edu)

Thematic Mapper (TM) imagery of two Central American volcanoes which have an array of lava units of known ages were studied to evaluate the utility of TM data for mapping at tropical volcanoes. We studied images of Izalco Volcano in El Salvador and Santiaguito Volcano in Guatemala. Izalco is a basaltic volcano in a moderately humid climate with units ranging from 25 to 200 years in age, while Santiaguito is a dacitic volcano in a very humid climate with units ranging from <1 to 70 years. Both are well mapped, and the ages of principal lava units are well known. The TM study allows the discrimination of units with known ages, using a variety of image processing classifications. We present the results based on image processing and compare it with maps from geologic observations to show that TM can make a strong contribution to mapping efforts at tropical volcanoes with very recent activity. The results were supplemented with field ground truth measurements using a spectrometer which collected spectra from 300 to 900 nm, covering the TM bands 1-4 for specific field sites, allowing us to examine the spectral effects of regenerating vegetation at Santiaguito, and to compare the ground truth data with comparable regions in the TM image. These results also demonstrate spectral changes associated with morning solar warming, showing that there are large changes in spectra over the period of 8-10 AM local time when TM data are typically collected over Central America.

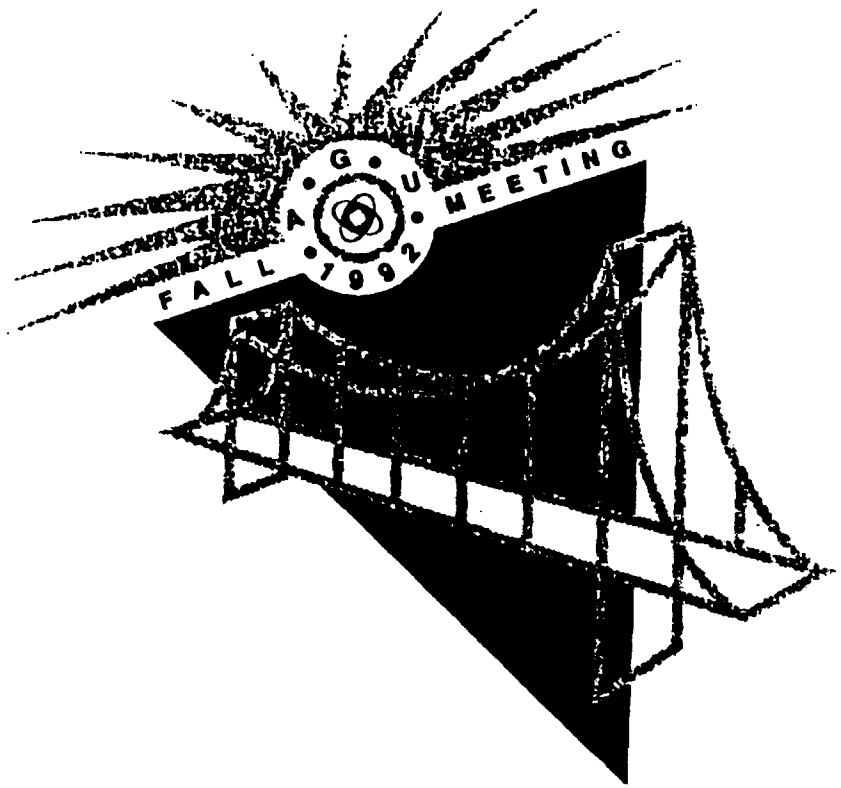

Automatic Volcanic Cloud Mapping using AVHRR

William I. Rose and David J. Schneider (Geological Engineering, Michigan Technological University, Houghton, MI 49931; 906-487-2531; E-mail: raman@mtu.edu)

Multispectral image processing of AVHRR (Advanced Very High Resolution Radiometer) data has succeeded in discriminating eruption clouds from weather clouds in a number of circumstances (Hanstrum and Watson, 1983, *Austral. Met. Mag., 31: 171-177*; Prata, 1989, *Int. J. Rem. Sens. 10: 751-761*; Holasek and Rose, 1991, *Bull. Volc., 53: 420-435*). Perfection of techniques could lead to real time operational use in reducing dangerous aircraft encounters with volcanic clouds and we have continued to investigate images from archived NOAA data in order to develop a procedure that could be automated. We have now studied a variety of different eruptions which exhibit a large range of volcanic and atmospheric conditions. No one algorithm can be used for successful discrimination for all examples studied so far. We do not understand enough about which variables (cloud temperature, temperature contrast between the cloud and the underlying surface, ash content of cloud, water vapor content of cloud, sizes of ash particles, etc.) influence the spectral responses observed in the plumes to devise a systematic automatic procedure. Our goal is to develop an automatic method, but the complexity of the problem may require us to perform laboratory spectrometric measurements of ash and aerosols, and to do particle sampling of actual eruption clouds which are simultaneously imaged, in order to be certain that we do not overlook the robust range of possible eruptions and environmental conditions. The presentation will illustrate the problems of automation with examples of AVHRR volcano images studied in detail.

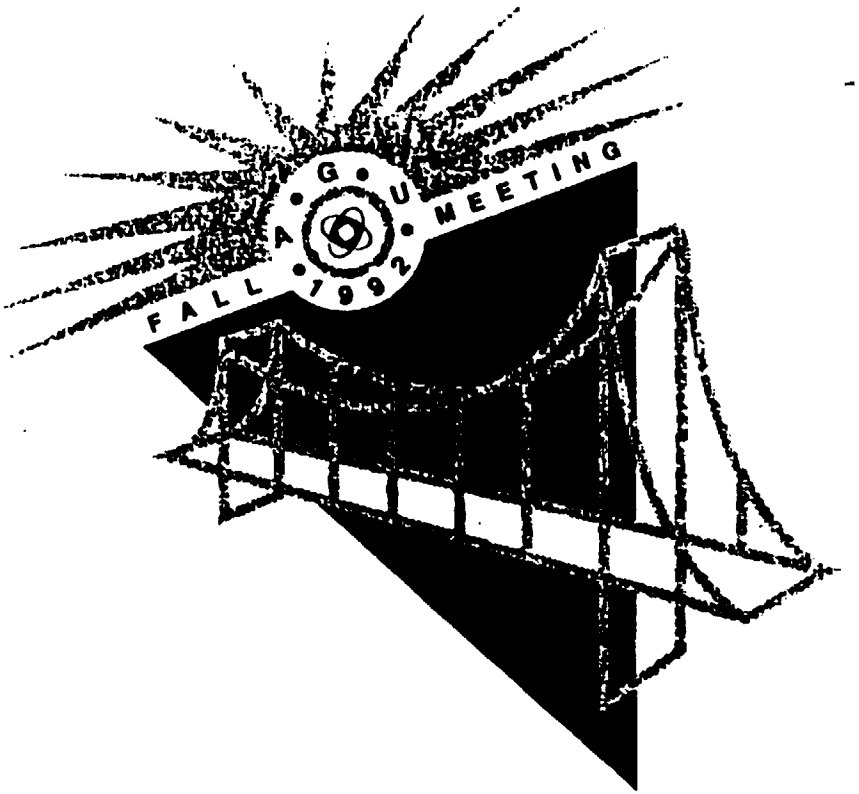

FEDERAL AVIATION ADMINISTRATION

WORKSHOP ON OLD

VOLCANIC ASH CLOUDS

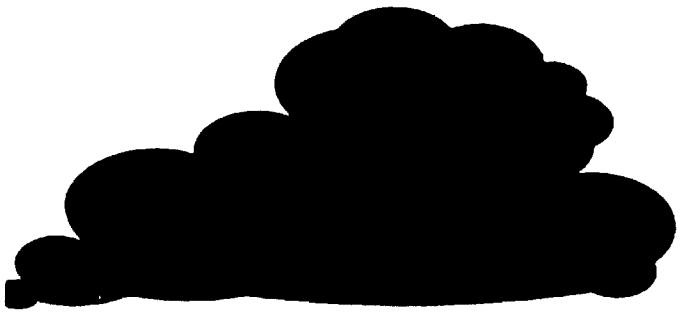

WASHINGTON, D.C.
APRIL 22-23, 1993

POSSIBLE USE OF AVHRR FOR DETERMININGASH BURDENS IN VOLCANIC CLOUDS: PRELIMINARYWORK ON CRATER PEAK/SPURR DATA

William I. Rose, David J. Schneider and Shimeng Wen
Michigan Technological University
TEL:906/487-2531; FAX: 906/487-3371

Lee Kelley
National Weather Service

The three 1992 Crater Peak/Spurr eruptions provided a robust test of new HRPT Information Processing System installed in Anchorage for real-time tracking of the volcanic clouds. The system uses AVHRR satellite images and processes them using multispectral techniques. The Spurr eruptions produced clouds that were prominent and which could be tracked for thousands of kilometers. We present many examples of processed imagery, which reflects the real-time capability now available. The frequency of imagery (about once every few hours) allows for a clearer understanding of the patterns of change in spectral response that occur during the evolution of a volcanic cloud. The images taken during eruption and shortly thereafter are apparently very rich in water droplets and/or ice, which makes the spectral signal very much like a meteorological cloud. Within a few hours, the clouds change spectrally, first at the edges, then throughout, so that they can be distinguished easily using an apparent temperature difference determined from data in spectral bands 4 and 5 of the AVHRR. The clouds can be tracked for at least 80 hours after eruption, using the apparent temperature difference technique, during which they travel thousands of kilometers, and the signal determined from the apparent temperature differences decays. One principal objective is to mitigate hazard to aviation. Two of the three Spurr clouds traveled southward, over the continental US. Drifting volcanic clouds may be hazardous to aircraft for 24 hours or more after eruption. In view of the need to alleviate potential hazard to aviation, it is important to quantify the apparent temperature difference signal we can measure with ash concentration, and to learn how to measure when such drifting volcanic clouds are hazardous to aircraft. We have done initial theoretical radiative transfer calculations and applied a multispectral retrieval model to AVHRR data to obtain particle size, emissivity, transparency, optical depth, and particle burden. These calculations are compared with actual data from the Spurr clouds, which demonstrate the possible efficacy of the method. If the method can be tested and perfected, it can form the basis for satellite-based assessment of silicate burdens of ash clouds. Such data are fundamental for assessing the aircraft hazard of "old ash clouds".

Satellite-Based Estimates of Ash Content of Drifting Volcanic Clouds

W I Rose (Geological Engineering, Michigan Tech Univ, Houghton, MI 49931; 906 487-2531; e-mail: raman@mtu.edu) S. Wen, D. J. Schneider

Over the past year we have developed a radiative transfer model that can retreive particle sizes, optical depth and particle masses in transparent volcanic clouds (Wen and Rose, this meeting) using two bands of thermal infrared data from the AVHRR. The method is a new tool to examine the fate and transport of volcanic ash in earth's atmosphere. The two band AVHRR method can be applied to a 15 year archive of data on volcanic clouds beginning in 1978. We expect that the results will help us measure the total volumes of eruptions, by facilitating measurement of far flung ash. The study of multiple images from the same eruption will enable study of dispersion and particle fallout over the first days of the drifting cloud (Schneider et al, this meeting). More robust methods expanding the same ideas to multiple thermal infrared bands are being developed using the TIMS, MODIS and ASTER sensors. These methods will be overdetermined and will allow us to refine the techniques considerably. We have also begun study of simultaneous data on volcanic clouds collected by AVHRR and TOMS, using processed data obtained from the TOMS investigators at NASA Goddard (Hossli et al, this meeting). Because the AVHRR detects ash, and the TOMS detects SO_2, using both sensors potentially allows us to see the separation of ash and SO_2.

1993
AGU FALL MEETING
December 6–10,
San Francisco, California

FEDERAL AVIATION ADMINISTRATION

WORKSHOP ON OLD VOLCANIC ASH CLOUDS

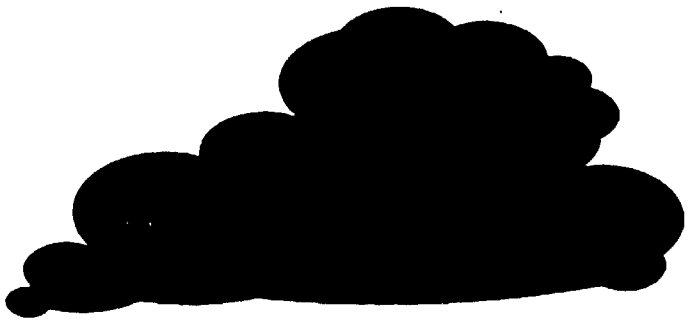

WASHINGTON, D.C.
APRIL 22-23, 1993

AVHRR OBSERVATIONS OF THE VOLCANIC ASH CLOUD FROM PINATUBO VOLCANO

David J. Schneider and William Rose
Michigan Technological University
TEL: 906/487-2531; FAX: 906/487-3371

The June 15, 1991, eruption of Pinatubo Volcano produced a large ash cloud which drifted for thousands of kilometers. Casadevall (*Aviation Safety Journal, v. 3, no.2, pp.3-11*) reported that 17 commercial aircraft were damaged by in-flight encounters with ash from Pinatubo, and that world-wide, more than 50 aircraft have been damageed by encounters over the past 12 years. Satellite observations of volcanic clouds have the potential to reduce these dangerous and costly encounters. More than 20 Advanced Very High Resolution Radiometer (AVHRR) images between June 12 and June 20, 1991 have been analyzed. Volcanic clouds were successfully discriminated from meteorological clouds in the images by calculating an AVHRR band 4-minus-band-5 temperature difference. From June 12 to June 16, the boundaries of the volcanic clouds as discriminated by the band-4-minus-5 operation were correlated to cold clouds observed in band 4-images, such as those now used routinely in meteorological analyses. However, by June 17, the boundary of the volcanic cloud could not be identified in the band 4-images. Because the main mass of volcanic material was transported in the stratosphere, its movement is unrelated to the movement of tropospheric clouds. In cases like these, multispectral image processing is the only way to determine the boundaries of the volcanic cloud. The magnitude of the band-4-minus-5 volcanic-ash signal declined over time, possibly due to the fallout of ash particles and the dispersal of the cloud. We hope to invert the bispectral AVHRR data to estimate particle size and concentration.

Eruption cloud opacity related to particle mass concentration, size distribution and wavelength

Zhenni Wang, William I. Rose and Alexander Kostinski
(Michigan Technological University, Houghton, MI 49931; 906-487-2531; E-mail: raman@mtu.edu)

Volcanic clouds are partly opaque and partly transparent when detected by satellite remote sensors. We have investigated the theoretical conditions in which light transmission through volcanic clouds occurs by applying Mie theory methods described by Thielke and Pilat (*Atmos. Env., 12:* 2439-2447). In this initial effort we are determining theoretical results that describe the pattern of transmittance as a function of concentration, and particle size distribution for volcanic ash clouds at wavelengths that ranging from visible to thermal infrared. We are motivated by the possibility that multispectral satellite imagery of ash clouds, particularly when they are carried over spatially homogeneous surfaces such as seas, can yield differential transparency at different wavelengths, that if understood, can map particle concentrations and size information in satellite images.

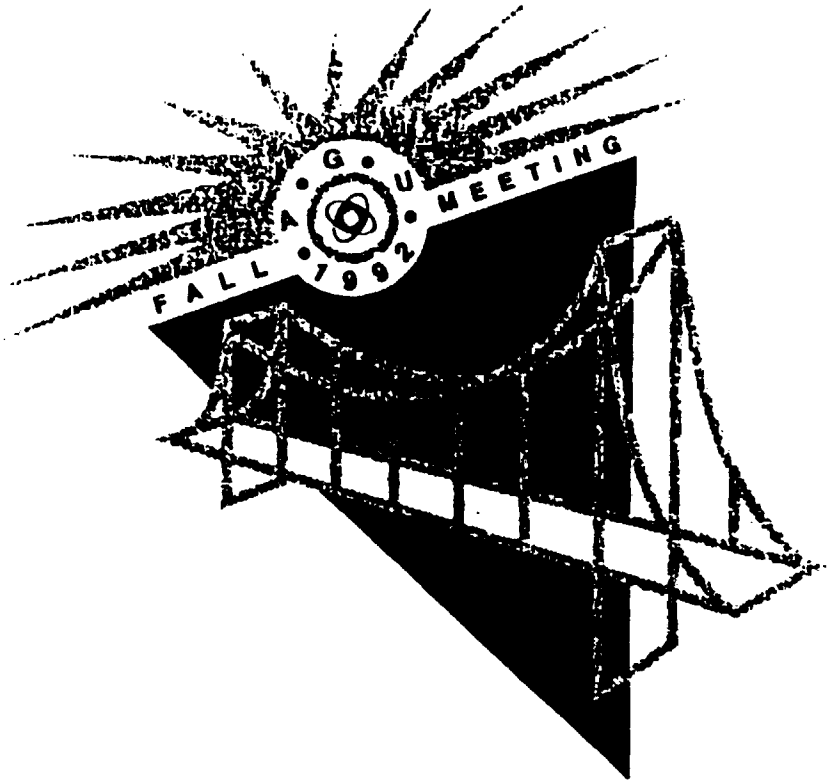

RETRIEVAL OF PARTICLE SIZES AND MASSES IN VOLCANIC CLOUDS USING AVHRR BANDS 4 AND 5

Shiming Wen and William I. Rose

Department of Geological Engineering, Geology and Geophysics
Michigan Technological University
Houghton, MI 49931

Submitted for publication to JGR-Atmospheres: August 23, 1993

Retrieval of Particle Sizes and Masses in Volcanic Clouds Using AVHRR Bands 4 and 5

Shiming Wen and William I. Rose

Department of Geological Engineering, Geology and Geophysics
Michigan Technological University
Houghton, MI 49931

ABSTRACT

The AVHRR sensor on polar orbiting NOAA satellites can discriminate between volcanic clouds and meteorological ones using two-band data in the thermal infrared. This paper is aimed at developing a retrieval of the particle sizes, optical depth and particle masses from AVHRR two-band data of volcanic clouds. Radiative transfer calculations are used with a transparent cloud model that is based on assumptions of spherical particle shape, a homogeneous underlying surface and a simple thin cloud parallel to the surface. The model is applied to observed AVHRR data from a 13 hour old drifting cloud from the 19 August 1992 eruption of Crater Peak/Spurr Volcano, Alaska. The AVHRR data fit in the range of results calculated by the model, which supports its credibility. According to the model results, the average of effective particle radius in the test frame of this cloud is in the range of 2 to 2.5 μm, the effective emissivity averages 0.6 and the optical depth is about 0.60 - 0.65. The mass of ash estimated amounts to 35,000 -50,000 tons in the test frame of the cloud, and to 0.20 - 0.28 x 10^6 tons in the whole cloud. The total estimated mass is about 0.5-0.8% of the mass measured in the ashfall blanket. Applications of the new retrieval method are listed.

INTRODUCTION

Measuring the size and burden of silicates and other components in volcanic clouds is of interest to those studying volcano atmosphere interactions (Table 1). Weather

satellites have been a useful way to track drifting volcanic clouds (Hanstrum and Watson, 1983; Sawada, 1987) and two-band processing of thermal infrared data from weather satellites has allowed for the discrimination of volcanic and meteorological clouds (Prata,1989a; Holasek and Rose, 1991). The explanation of the cause of infrared two-band discrimination and volcanic clouds have been discussed by Prata (1989a, 1989b), Holasek and Rose (1991) and Schneider and Rose (1993), and is the result of scattering and absorption of thermal emission from matter underneath the volcanic cloud by the cloud itself. In this paper we develop a model of radiative transfer to attempt to retrieve the particle sizes and masses of particles in drifting volcanic clouds. The model builds on work of Prata (1989b) on volcanic clouds, on methodology published by Yamanouchi et al (1987), and on cloud retrieval methods of Lin and Coakley (1993). We compare our method with actual data on the Crater Peak/Spurr eruption of 19 August 1992 to begin to evaluate the model, and discuss some of the uncertainties and applications.

BASIC THEORY

Radiative transfer calculations have been used to develop two-band models for retrieving the optical parameters of clouds, such as particle sizes, emissivity, transmissivity, and cloud cover, because radiance attenuation through the atmosphere functionally depends on geometrical and optical properties of the clouds in the process of radiative transfer. The observed radiances by a satellite-based remote sensor through a transparent cloud is composed of two parts, i.e., radiance from the clouds and from the underlying surface. Generally, if the fraction of partial cloud cover in a field of view is taken into account (Coakley,1983; Lin and Coakley; 1993), a linear model is valid under the following assumptions: (1) the cloud approximates a planar homogeneous cloud layer parallel to the surface (or a single-layer cloud system); (2) the background surface is homogenous; and (3) the atmosphere above the cloud and between the surface and the cloud are clear windows. In this case the observed radiance I_i in a narrow band i centered at wavelength λ_i is given by the following equation:

$$I_i = (1-A_c)\,B(T_s) + A_c(\varepsilon_i B(T_c) + t_i B(T_s)) \qquad (1)$$

where T_s is the brightness temperatures of the surface, T_c the temperature of the top of the cloud, B the Plank function, A_c the fraction of the clouds in the field of view, ε_i the emissivity, and t_i transmissivity of the clouds. The pixels are partially covered by clouds if A_c is less than 1. If the clouds are optically thick and completely overcast (ε_i=constant and A_c=1), the measured radiance I_i approximately equals to $B(T_c)$. On the other hand, for a partially transparent cloud layer overlying a warm surface ($B(T_s) >> B(T_c)$), the radiance (I_i) approaches $t_i B(T_s)$ as ε_i, a measure of the transparency, approaches 0.

Radiative Transfer Equation

To obtain the theoretical radiance defined in equation (1), the radiative transfer calculation has to be used because of unknown emissivity and transmissivity at different wavelengths. The radiative transfer equation for a scattering plane parallel atmosphere is given by:

$$\mu \frac{\partial I}{\partial \tau}(\tau, \mu, \phi) = I(\tau, \mu, \phi) - J(\tau, \mu, \phi) \qquad (2)$$

$J(\tau,\mu,\phi)$ is the source function given by

$$J(\tau, \mu, \phi) = \frac{\omega}{4\pi}\int_0^{2\pi}\int_{-1}^{1} P(\mu, \phi; \mu', \phi') \times I(\tau, \mu', \phi')\, d\mu'\, d\phi' + \frac{\omega F_\odot}{4} P(\mu, \phi; \mu_o, \phi_o)\, e^{-\tau/\mu_o}$$

where I is the diffuse radiance, $\pi F_\odot$ incident solar flux, τ the optical depth, μ the cosine of the zenith angle, ω the single scattering albedo is defined as the radio of scattering cross section σ_s to extinction (scattering plus absorption) cross section σ_e, μ_o the cosine of the solar zenith angle, and $P(\mu,\phi;\mu',\phi')$ is the axially-symmetric phase function defining the light incident at μ', ϕ' which is scattered in the direction μ, ϕ. The single-scattering albedo, phase function, and extinction cross section are functions of the incident wavelength, particle size and shape, and refractive index. In the 10-12 μm region, the

source due to incident sunlight, i.e. the last term $Q=(1/4)\omega F_0 P(\mu,\phi;\mu_0,\phi_0)e^{-\tau/\mu_0}$ subscript 0, is negligible compared with radiation due to emission.

Eddington's Approximation

To solve equation (2), several methods have been developed, such as Discrete-ordinates method (Chandrasekhar, 1960; Liou, 1973), Adding method (van de Hulst, 1980), Monte Carlo method, Doubling method, Two-stream and Eddington's approximation (Eddington, 1916). Here Eddington's approximation was used because it is a good approximations for thick layers (Liou, 1992) and offers a way to rapidly compute irradiances with an accuracy of several percent (Shettle and Weinman, 1970). Eddington's approximation assumes that the radiance can be simply approximated by a linear function

$$I(\tau,\mu)=I_0(\tau)+I_1(\tau)\mu \tag{3}$$

and the phase function can be approximated by

$$P(\mu,\mu')=1+3g\mu\mu' \tag{4}$$

where the asymmetric parameter $g=(1/2)\int P(\theta)\cos\theta d(\cos\theta)$ (θ is the angle between incident and scattered radiances) is a measure of the amount of radiation scattered toward the Earth's surface relative to that scattered back to space.

If an atmosphere composed of homogeneous layers is assumed, we have $\partial\omega/\partial\tau=\partial g/\partial\tau=0$, and straightforward analyses yield the following solution:

$$I_0=Ae^{-k\tau}+Be^{+k\tau} \tag{5}$$

$$I_1=-\sqrt{\frac{3(1-\omega)}{1-\omega g}}Ae^{-k\tau}+\sqrt{\frac{3(1-\omega)}{1-\omega g}}Be^{+k\tau} \tag{6}$$

Therefore, the downward (F^-) and upward (F^+) flux are given by

$$F^-(\tau) = 2\int_{-1}^{0} \mu I(\mu)\, d\mu = -(1+U)Ae^{-k\tau} - (1-U)Be^{+k\tau} \quad (7)$$

$$F^+(\tau) = 2\int_{0}^{1} \mu I(\mu)\, d\mu = (1-U)Ae^{-k\tau} + (1+U)Be^{+k\tau} \quad (8)$$

where $k=[(1-\omega)(1-\omega g)]^{1/2}$ and $U=[4(1-\omega)/3(1-\omega g)]^{1/2}$.

For the boundary condition for a homogenous parallel cloud, it is assumed that the medium is only illuminated from above by a known source of radiation:

$$F^-(0) = -F_o, \qquad F^+(\tau_c) = 0.$$

From this boundary condition, coefficients A and B can be determined.

From above, the reflectivity of the atmosphere (R) is the proportion of reflective flux at the top of the atmosphere to the incident flux, and the transmissivity of the atmosphere is the proportion of transmitted flux to incident flux, i.e.,

$$R = \frac{F^+(0)}{F_o} = \frac{(1-U^2)(e^{-k\tau_c} - e^{+k\tau_c})}{(1-U)^2 e^{-k\tau_c} - (1+U)^2 e^{+k\tau_c}} \quad (9)$$

$$T = \frac{F^-(\tau_c)}{F_o} = \frac{4U}{(1-U)^2 e^{-k\tau_c} - (1+U)^2 e^{+k\tau_c}} \quad (10)$$

and emissivity $E=1-R-T$.

TEMPERATURE DIFFERENCE MODEL

Prata (1989b), Wu (1987), and Yamanouchi et al. (1987) applied the temperature difference method to retrieve weather cloud parameters for complete cloud cover. In fact, the radiative calculation for the temperature difference method is a special case of equation (1) under the assumption $A_c=1$. The study frame selected (see below, Fig. 4) is located in the center of cloud image, and the pixels of the frame can be reasonably

considered as complete cloud cover, but still partially transparent.

Band 4 (10.3 -11.3 μm) and band 5 (11.5 - 12.5 μm) of AVHRR are used in our temperature difference model, because the temperature difference of band 4 and band 5 (T_4 - T_5) is a fairly reliable criterion used to distinguish meteorological clouds and volcanic clouds. When a volcanic cloud exists, T_4- T_5 is usually < 0, otherwise T_4 - T_5 >0 (Prata, 1989a; Schneider et al., 1993).

The purpose of the Temperature Difference Model (TDM) proposed here is to estimate the mass of particles in volcanic clouds. So two parameters, particle radius and optical depth, are essential in this model. The radiative transfer model is based on the following assumptions: (1) the shape of the volcanic particles is spherical, therefore Mie theory can be used to calculate extinction cross section (σ_e), asymmetric parameter (g), and the single scattering albedo (ω) for a known refractive index (which depends on wavelength and composition) and particle radius; (2) the particle size distribution, $n(r)$, is uniform within each pixel; and (3) the volcanic clouds are continuous, i.e. A_c=1. Based on assumption (3), (1) can be expressed as:

$$I_i=(1-R_i(r_e,\tau_c))B(T_c)+t_i(r_e,\tau_c)(B(T_s)-B(T_c)) \quad (11)$$

where r_e is the effective radius of the spherical particle for given size distribution $n(r)$, i.e.

$$r_e=\frac{\int \pi r^3 n(r)\,dr}{\int \pi r^2 n(r)\,dr} \quad (12)$$

and τ_c is the optical depth defined by

$$\tau_c=L\cdot\int Q_{ext}\pi r^2 n(r)\,dr \quad (13)$$

where L is the geometric thickness of the clouds, Q_{ext} is the efficiency extinction factor calculated by Mie theory, and $\sigma_e=\pi r^2 Q_{ext}$ is extinction cross section.

Once the simultaneous pairs of radiance (I_i, I_j) are calculated for varying r_e and τ_c, the corresponding brightness temperature pairs (T_i, T_j) can be obtained by the rearranged version of Plank's formula:

$$T_i = \frac{1.43879\times10^4}{\lambda_i \ln([3.74151\times10^8\lambda_i^{-5}/\pi I_i]+1)} \qquad (14)$$

where λ_i is wavelength in microns.

Theoretical calculations based on the model are shown in Figure 1, where the solid lines represent the effective radius of volcanic ash particles and dashed lines represent the 10.8 μm (band4) optical depth of the cloud. The model reveals a nonlinear relationship of temperature difference with brightness temperature due to the nonlinear relation of optical depth with wavelengths. The theoretical calculation shows that the lowest temperature difference (LTD) of band 4 and band 5 linearly depends on the temperature difference of the cloud top and the surface (T_s - Tc), i.e., when T_s -T_c increase, LTD will linearly increase. If the surface temperature T_s is 273°K and the cloud top is 213°K (the conditions of our test data set), LTD cannot be lower than -30°C, and the brightness temperature corresponding to LTD is about 227°K. It is found that the characteristics of negative temperature difference will disappear completely if the particle size is greater than 5 μm (see fig. 1).

In figure 1, let $S(r_e)$ be a variable that records the size of area embraced by the straight line which presents the appearance of 0 degree temperature difference and the curved line which represent the change of the temperature pairs (T_4 , T_4- T_5) along with varying degree of transparency at different effective radii r_e. So S is a function of r_e. A plot of normalized S (maximum S is assigned to 1) versus the particle radius (r_e) shows in Figure 2. $S(r_e)$ is a parameter that presents the retrieval sensitivity of the effective radius. If S is a monotonic function, then the observed temperature pairs (T_4, T_4 - T_5) can be *uniquely* related to effective radius and optical depth pairs (r_e, τ_c) . In our example (fig. 2), $S(r_e)$ is a monotonically decreasing function in this interval from 0.8 to 4.3 μm.

STUDY CASE

As an initial test for our model we examined volcanic cloud data taken from the August 19, 1992 Crater Peak/Spurr eruption . Nine digital images of AVHRR were received from the NOAA 11 and 12 polar orbiting satellites. Previous study (Schneider et al, 1993) indicates that the images taken early in the eruption are apparently very rich in water droplets and/or ice and of large particle size. This makes the spectral signal similar to a meteorological cloud. However, when the drifting volcanic clouds dry out and the particle size becomes small during transport and dispersion, the clouds take on spectral properties dominated by fine volcanic ash. For the purpose of this study, the selected data was taken at 1338 GMT on August 19, 1992, about 13 hours after the onset of the eruption and 9 hours after it ended. At this point the cloud was located over the Gulf of Alaska, more than 300 km from Spurr Volcano. We used a sample frame of 1.1 km resolution Local Area Coverage (LAC) data of cloud surface temperatures of band 4 and band 5. In the sample frame, composed of 150 × 100 pixels, covering an area of about 18150 km^2, the volcanic clouds overlapped low-level meteorological clouds (Figure 3).

Parameter selection

In this study, we don't have refractive index directly measured from Spurr ash. We assume that the volcanic clouds contain only volcanic ash and we used refractive index data on ash obtained by Volz (1973) and Pollack, Toon et al.. (1973). The six samples provide a good variety of volcanic ash types with crystalline andesite, crystalline basalt, glassy basalt, and glassy rhyolites (table2). The composition of Crater Peak/Spurr eruption is andesite, similar to sample 1, therefore we focus the refractive index of sample 1 and test the sensitivity of refractive index by comparing results using the other samples.

The cloud top temperature (T_c) is chosen at 213°K, which is determined by the coldest part of the earlier images of the volcanic clouds, where the absolute temperature difference between band 4 and band 5 is less than 0.5°C. The surface temperature (T_s) is chosen 273° K, which is determined from the band 4 and band 5 calibrations based on observations of areas, that surround the volcanic cloud in the AVHRR images, which are

free of meteorological clouds, except for the homogeneous low deck of clouds that underly the volcanic cloud.

Retrieval of particle sizes and optical depths

Figure 4 shows results obtained from actual pixels in the sample frame superimposed on the calculated curves of figure 1. Most of points in the frame cluster between particle sizes of 1 and 4 μm (figure 4). To understand the spatial distribution of effective radiance, twenty theoretical curves from 0.5 to 5 μm with increments of 0.25 μm were calculated to analyze the AVHRR data in more detail. The minimum effective radius is selected to be 0.5 μm rather than 0 because of the existence of multiple solutions of our model for radius less than 0.8 μm (note the non-decreasing function $S(r_e)$ fraction of Figure 2). The frequency distribution shows pixels with an effective radius of less than 0.8 μm are only 1.36% of the total pixels, and the mean radius and standard deviation are 2.67 μm and 0.58, respectively (Figure 5). Mapping effective radii allows examination of the spatial distribution of particle size (Figure 6). The contour map shows that the effective particle sizes in the frame vary from 2.5 and 3 μm at the center, to between 3 and 4 μm in the west, and to between 2 and 1.5 μm in the east. There is a dramatic difference in particle size at the east and west edges of the frame (also the edges of the clouds), and the center is relatively homogenous (also the center of clouds). This variation could be due to changes in cloud altitude with dispersal as volcanic ash particles are being fractionated. A possible explanation consistent with the observed data is that the eastern edge of the cloud is higher and has moved faster than the western edge. It is also possible that at the edges of the cloud, the assumption of continuous coverage is violated, which gives us spurious results.

The spatial distribution of optical depths of band 4 is shown in Figure 7, where twenty curves of optical depth with increments of 0.1 are calculated for retrieval. The optical depth in the sample test frame varies from 0.1 to 1.25, the mean value is 0.65 and standard deviation 0.28. The largest values of optical depth appear at the center of the

clouds, and the smallest ones are at the cloud edges.

Estimation of the total mass

Using a density of 2.6g cm^{-3} (Neal et al, in press) for the volcanic particles, the total mass of the frame is the accumulation of pixel-scale mass, i.e.

$$M_{total}=\sum_{i=1}^{100}\sum_{j=1}^{150} L^{(i,j)} S\cdot \rho\int\frac{4}{3}\pi r^3 n(r)\,dr$$

$$=\sum_{i=1}^{100}\sum_{j=1}^{150} 1.21\times\frac{4}{3}\rho r_r^{(i,j)}\tau^{(i,j)}\frac{\int\pi r^2 n(r)\,dr}{\int Q_{ext}\pi r^2 n(r)\,dr} \qquad (ton) \quad (15)$$

where $\rho(g/cm^3)$ is particle density, $r_e^{(i,j)}$ (μm), and $\tau^{(i,j)}$ are retrieval effective radius and optical depth of pixel (i,j), respectively. $L^{(i,j)}$ is geometric thickness of pixel (i,j), and S is the area of each pixel. If the particle distribution $n(r)$ reduces to uniform distribution, i.e. $n(r)=1$, then the inner term of the above sum simply becomes $1.21\times4/3\times\rho r_e^{(i,j)}\tau^{(i,j)}/Q_{ext}(r_e^{(i,j)})$. The Q_{ext} at different effective radius are listed in table 3.

Using the retrieval of $r_e^{(i,j)}$, $\tau^{(i,j)}$ and Q_{ext} discussed above, the total mass of volcanic ash in the study frame is about 36,200 tons. By extending the result to the whole cloud (about 100,000 km^2 in total area, see figure 4), the total mass is about 0.2×10^6 tons, which is about 0.56% of the total volcanic ash measured in the deposited ash blanket (36×10^6 tons) (Neal et al, in press).

Since we have little direct information for the size distribution of the study cloud, the above estimation is simply based on the assumption of uniform size distribution. Our later work shows that there is no big change for the total mass due to several possible size distributions. This will be discussed in the next section.

CONCLUSIONS AND DISCUSSIONS

Theoretical study and application to a volcanic cloud imaged by AVHRR radiative transfer calculations in the infrared window channels can be used to retrieve the effective

radius of volcanic ash particles and optical depths of clouds from AVHRR multispectral images. The major conclusions from this study are:

(1) Volcanic clouds have negative brightness temperature differences (band 4 - band 5) only if they have a dominance of particles with radius less than 5 μm.

(2) Our model works best when there is large difference between the temperature of the underlying surface and the volcanic cloud. The lowest temperature difference (band 4 - band 5) of the volcanic cloud is a linear function of the temperature difference between the underlying surface and the volcanic clouds (T_s - T_c).

(3) This method can be used to interpret volcanic clouds with a dominant effective radius between 0.8 and 4.3 μm.

(4) The mean radius and the optical depths within the test frame of a 13 hour old August 1992 Crater Peak/spurr volcanic clouds are determined to be 2.67 μm and 0.65, respectively, based on the two-band model. The estimate of the mass of the volcanic cloud particles is about 28 - 36 $\times 10^3$ tons in the frame, and about 0.15 - 0.2x10^6 tons in the whole cloud, which is about 0.4 - 0.56% of the total volcanic ash measured in the ash blanket (36x10^6 tons).

The temperature difference model for a homogenous parallel cloud is completely controlled by the refractive index of particles in the cloud (which is dependent on their chemical composition, environmental variables T_s and T_c, the shape of the particles, and the size distribution of particles). Uncertainties in any of these parameters will influence the accuracy of the retrieval. At least for the Spurr cloud in our study, the model gives reasonable results (Figures 4-8). Additional studies of other volcanic clouds are needed to validate the model and to determine the conditions which favor accurate retrievals.

Uncertainty about refractive index of volcanic ash

In order to investigate the sensitivity of our model to uncertainty about refractive index, we compared results using the data from a variety of samples (figure 8; table 4).

Some of the refractive index data (sample 4, 5 and 6) cause pixel points to fall outside of the fields of calculated results, we interpret this to reflect a lack of similarity in composition for those samples to the Spurr ash. For the three samples that do match spurr well, the effective radius determined ranges from 2 to 2.6 μm,the optical depth from 0.6 to 0.67 and the mass in the frame from 28,000 to 36,000 tons. It would obviously be desirable to have refractive index data on the Spurr ash, but the sensitivity of this uncertainty is not too serious at this point.

Silicates and sulfuric acid aerosols

Silicates (volcanic ash) and sulfuric acid aerosol particles are both found in volcanic ash clouds (Rose et al., 1980; 1987; Tabazedeh and Turco, 1993). Prata (1989a) showed that either silicates or sulfuric acid can produce negative apparent temperature differences. We used refractive index data for sulfuric acid aerosols (Halperin and Murcray, 1987) to calculate model results analogous to those for silicates, for a variety of dilutions of H_2SO_4. Results show that aerosol with >50% H_2SO_4 are indistinguishable from silicates with two-band AVHRR retrievals. The possible confusion of the two types of particles depends partly on the age of the volcanic cloud because ash is the dominant particle component of young ash clouds (Rose et al., 1980, 1987), but is removed from the atmosphere relatively quickly, in days to months (Turco et al., 1983; Pinto et al., 1989) while volcanic sulfuric acid may persist in the atmosphere for several years (Rampino et al., 1988; Bernard and Rose, 1989). For the Spurr cloud we used in our study, silicates probably exceed sulfuric acid particles by orders of magnitude. After atmospheric residence times of a week or more, confusion between the two particles types would be more of an issue. We have begun to investigate where three-band retrievals, involving band 3 of AVHRR (3.5 μm), can be used to distinguish between concentrated H_2SO_4 and silicate components, it may also open the range of retrievable sizes, but the intensity of band 3 radiation in nighttime AVHRR may not be sufficient. During the day it is useless due to reflected solar.

Temperature difference between the volcanic cloud and the warmer subsurface

The retrieval model we have developed is highly sensitive to the temperature difference (T_s - T_c) between the warmer surface (land, sea or clouds) and the top of the volcanic cloud. We expect that (T_s - T_c) values will be typically positive, because tropospheric temperatures decrease rapidly with height and drifting volcanic cloud particles will equilibrate with the temperature of surrounding air. However the temperature of the surface can vary a lot, being highest on warm summer days in which there are no meteorological clouds (T_s - T_c up to as high as 100°C) and lowest on days when high cold clouds underlie the volcanic cloud or in winter and night when the surface temperatures may be much lower. This effect is shown by comparing Figure 9 with Figure 1, which helps explain why some AVHRR images are such more successful in mapping and discriminating volcanic clouds (Schneider et al., 1993) than others (Schneider and Rose, 1993).

Size distribution of particles

The mass calculation is obviously dependent on the size distribution of particles (note the equations (13),(14),and (16)). The assumed uniform distribution is undoubtedly too simple to be reliable. Two other size distributions, Gamma and Lognormal, were suggested by many authors based on experiments and measurements (Deirmen, 1969; Prata, 1978). From the measurements of particles in the 1990 volcanic clouds of Mount Redoubt (Hobbs et al., 1991), volcanic dust has Lognormal size distribution with parameters μ=-1.36, σ=0.74 and mean radius=0.808 μm. We assumed σ=0.74 in this study. Table 5 lists the comparison of the mass estimates based on different size distribution in the frame scale retrieval. It can be seen that the mass estimates vary only slightly from the uniform distribution for some possible gamma and lognormal distributions which could span the ranges of volcanic clouds, based on limited study of size distributions of particles by aircraft-based studies (Rose et al, 1980; Hobbs et al, 1991).

The table 5 implies the following conclusion: (1) when the variance increases in

size distributions, the estimated mass will increase, as well ; (2) when lognormal distribution is chosen, an effective radius of 2 to 2.6 μm equals to a lognormal average of particle radius of between 0.7 and 0.9 μm, which coincidentally matches the average radius (0.808 μm) of airborne measurement of 1990 Mount Redoubt eruption cloud (Hobbs et al., 1991) ; (3) when six refractive index samples are considered in lognormal size distribution, the estimated mass in the whole cloud is in the range of 280 - 290×10^3, i.e. about 0.78-0.80% of the total volcanic ash measured in the ash blanket. The smaller change of mass within the samples than within the distributions indicates that the size distribution which is used is more important than composition of the volcanic dust for mass estimation.

Spatial resolution

The method used in this study assumes that the volcanic cloud forms a well defined homogeneous single layer in each pixel. However, real volcanic clouds do not exactly meet this assumption. In fact, the particle size distribution in Figure 6 shows that cloud in the frame is not a single parallel layer, but probably has a range of altitudes. Therefore, the accuracy of retrieval will be improved by a higher spatial resolution of the remote sensor. A smaller sized pixel will reduce the effects of variable altitudes and the cloud within each pixel can be better approximated as a layer. Thus the use of LAC data (1.1 km resolution) may be significantly better than GAC (4 km resolution) AVHRR data.

ACKNOWLEDGEMENTS

Financial support for this paper came from NASA through a Volcano/Climate Program contract NAG 5-1838. The AVHRR data used was obtained in a study funded by UCAR in the COMET program and was aided by an interaction with David Schneider, Lee Kelley, Gary Hufford and the Anchorage National Weather Service Office. The radiative transfer work was stimulated by interaction with Joy Crisp and Dave Schneider. It was started by Zhenni Wang and received vital encouragement and advice as the result

of a discussion with Jim Coakley. We were greatly helped by interactions with Xijian Lin. Dave Schneider prepared table 1 in the paper and helped preparing one of the figures. We appreciate the comments of reviews by Joy Crisp and Jim Coakley.

REFERENCES

Bernard, A. and W.I. Rose, 1990: The injection of sulfuric acid aerosols in the stratosphere by El Chichon Volcano and its related hazards to the international air traffic. Natural Hazards, 3, 59-67.

Chandrasekhar, S., 1960: Radiative Transfer. New York, Dover, 393 pp.

Coakley, J.A., Jr., 1983: Properties of multilayered cloud systems from satellite imagery. J. Geophys. Res., 88, 10818-10828.

Eddington, A.S., 1916: On the radiative equilibrium of the stars. Mon. Not. Roy. Astronom. Soc., 77, 16-35.

Halperin, B. and D.G. Murcray, 1987: Effect of volcanic aerosols on stratospheric radiance at wavelengths between 8 and 13 μm. Applied Optics, 26(11), 2222-2235.

Hanstrum B.N. and A.S. Watson, 1983: A case study of two eruptions of Mount Galunggung and an investigation of volcanic cloud characteristics using remote sensing techniques. Austral Meteorol Mag, 31, 171-177

Harris, D.M. and W.I. Rose, Jr., 1983: Estimating particle sizes, concentrations, and total mass of ash in volcanic clouds using weather radar. J. Geophys. Res., 88, 10969-10983.

Hobbs, P.V., L.F. Radke, j.h. Lyons, R.J. Ferck and D.J. Coffman, 1991: Airborne measurements of particle and gas emissions from the 1990 volcanic eruptions of mount redoubt, J. Geophys. Res, 96, 18735-18752.

Holasek, R.E. and W.I. Rose, 1991: Anatomy of 1986 Augustine Volcano eruptions as revealed by digital AVHRR satellite imagery. Bull. Volcanol., 53, 420-435.

Inoue, Toshiro, 1985: On the temperature and effective emissivity determination of semi-transparent cirrus clouds by bi-spectral measurements in the 10 μm window region. J. Meteor. Sci. Japan, 63, 88-98.

Lin, X.J. and J.M. Coakley, Jr., 1993: Retrieval of properties for semitransparent clouds from multispectral infrared imagery data.. J. Geophys. Res, in press.

Liou, K.N., 1973: A numerical experiment on Chandrasekhar's discrete-ordinates method for radiative transfer: Application to cloudy and hazy atmospheres. J. Atmos. Sci., 30, 1303-1326.

Liou, K.N., 1992: Radiation and cloud processes in the atmosphere. Oxford University Press, Inc., 487 pp.

Neal C.A, R.G. McGimsey, C.A. Gardner, M.L. Harbin, and C.J. Nye, 1992: Tephra-fall from the 1992 eruptions of Crater Peak, Mount Spurr Volcano, AK: A preliminary report on distribution, stratigraphy and composition. U.S.G.S. Bull. (1992 Spurr eruptions) edit by T. Keith, in press.

Pinto, J.P., R.P. Turco and O.B. Toon, 1989: Self-limiting physical and chemical effects in volcanic eruption clouds. Journal of Geophysical Research, 94, 11165-11174.

Pmpino M.R., S. Self, and R.B Stothers, 1988: Volcanic winters. Ann Rev Earth Planet Sci., 16, 73-99.

Prata, A.J., 1989a: Observations of volcanic ash clouds in 10-12 μm window using AVHRR/2 data. International Journal of Remote Sensing, 10, 571-761.

Prata, A.J., 1989b: Infrared radiative transfer calculations for volcanic ash clouds. Geophysical Research Letters, 16(11), 1293-1296.

Rampino M.R., S. Self, and R.B Stothers, 1988: Volcanic winters. Ann Rev Earth Planet Sci., 16, 73-99.

Rose, W.I., Chuan, R.D. Cadle, and D.C. Woods, 1980: Small particles in volcanic eruption clouds. Amer. J. Sci., 280, 671-696.

Rose, W.I., 1987: Santa Maria, Guatemala: Bimodal soda-rich calcalkalic stratovolcono. J. Vocanol. Geotherm, Res., 33 (stoiber Vol.), 109.

Sawada, Y., 1987: Study on analysis of volcanic eruptions based on eruption cloud image data obtained by the geostationary Meteorological Satellite (GMS). Tech Rep Meteorol Res Inst (Japan) 22.

Schneider, D.J. and W.I Rose, 1993: Observations of the 1989-90 Redoubt Volcano eruption clouds using AVHRR satellite imagery, submitted to Proceedings of the First International Symposium on Volcanic Ash and Aviation Safety, in press.

Schneider, D.J., W.I. Rose and L. Kelley, 1993: Real time tracking of 1992 Crater Peak/Spurr eruption clouds using AVHRR. U.S.G.S. Prof Paper (Spurr 92) ed by T. Keith,

in press.

Shettle, E.P. and J.A. Weinman, 1970: The transfer of solar irradiance through inhomogeneous turbid atmospheres evaluated by Eddington's Approximation. J. Atmos. Sci., 47, 1048-1055.

Tabazadeh, A. and R.P. Turco, 1993: Stratospheric chlorine injection by volcanic eruptions: HC1 scavenging and implications for ozone. Sciences, 260, 1082-1086.

Turco, R.P., O.B. Toon, R.C. Whitten, P. Hamill and R.G. Keesee, 1983: The 1090 eruptions of Mount St. Helens: physical and chemical processes in the stratospheric clouds. Journal of Geophysical Research, 88, 5299-5313.

van de Hulst, H.C., 1980: Multiple light scattering. Tables, Formulas and Applications, Vols. 1 and 2. Academic Press, New York, 739 pp.

Volz, F.E., 1973: Infrared optical constants of ammonium sulfate, Sahara dust, volcanic pumice, and flyash. Appl. Opt., 12(3), 564-568.

Wu, M.L., 1987: A method for remote sensing the emissivity, fractional cloud cover and cloud top temperature of high-level, thin clouds. J. Climate Appl. Meteor., 26(2), 225-233.

Yamanouchi, T., K. Suzuki and S. Kawaguchi, 1987: Detection of clouds in Antarctica from infrared multispectral data of AVHRR. J. Meteor. Sci. Japan, 65(6), 949-962.

Yamanouchi, T. and S. Kawaghchi, 1992, Cloud distribution in the Antarctic from AVHRR data and radiation measurements at the surface. Int. J. Remote Sensing, 13(1), 111-127.

Table 1. Need for satellite data on volcanic silicates in the atmosphere

	References*
Eruption volume:	
measure amounts of fine particles	[1,2]
Gas volume versus magma volume:	
petrologic methods of estimating SO_2: "excess sulfur"	[3]
entrainment of H_2O: source of stratospheric water	
Fallout of fine particles:	
fallout models	
mechanisms of fallout	[4]
Interactions between silicates and eruption cloud gases:	
self-limiting effects: scavenging of chlorine and sulfur	[5-7]
separation of silicates and sulfate aerosols	[8,9]
comparisons to TOMS SO_2 measurements	[10]
Cloud height and eruption rate:	
interpretation of eruption activity	
evaluation of column models	[11-13]
Drifting volcanic clouds:	
input into trajectory models	[14,15]
hazardous aircraft encounters	[16]

* 1. Fierstein and Nathensen (1992); 2. Rose (in press); 3. Andres et al. (1991); 4. Sorem (1982); 5. Tabazadeh and Turco (1992); 6. Pinto et al. (1989); 7. Rose (1977); 8. Bernard and Rose (1990); 9. Turco et al. (1983); 10. Bluth et al. (1992) 11. Koyaguchi and Tokuno (1993); 12. Woods (1988); 13. Carey and Sparks (1986); 14. Schoeberl et al. (1993); 15. Danielson (1982); 16. Casadevall (ed.) (1991).

Table 2. Refractive index of different samples

Sample descriptions	Band4 (10.3-11.3 μm)		Band5 (11.5-12.5 μm)		Sources
	Real	Imaginary	Real	Imaginary	
(1) Andesite: 54.15% SiO_2.	2.0534	0.60897	1.8392	0.13786	Pollack Toon Khare (1973)
(2) Basalt: 53.25% SiO_2.	2.1848	0.48812	1.9051	0.14670	
(3) Basaltic Glass: 53.45% SiO_2.	2.1241	0.71211	2.0129	0.24037	
(4) Obsidian-little Glass, Mt. California, rhyolite, 73.45% SiO_2.	2.0085	0.27476	1.7281	0.18407	
(5) Obsidian-Lake County Oregon, rhyolite, 76.20% SiO_2.	2.0268	0.27882	1.7410	0.18462	
(6) Volcanic dust: two samples are averaged. The andesitic Irazu ash sampled during ashfall is dark grey with feldspar, and the Hawaii sample was lightly weathered vesicular basaltic glass.	1.7900	0.3700	1.8000	0.18000	Volz (1973)

Table 3. Efficiency extinction factors of 10.8 μm for volcanic ash

r_e(μm)	0.25	0.50	0.75	1.00	1.25	1.50	1.75	2.00	2.25	2.50
Q_{ext}	0.2446	0.4319	0.7135	1.1237	1.6561	2.2279	2.6945	2.9434	3.0155	2.4941
r_e(μm)	2.75	3.00	3.25	3.50	3.75	4.00	4.25	4.50	4.75	5.00
Q_{ext}	3.1076	3.1618	3.1522	3.0853	3.0111	2.9621	2.9321	2.8988	2.8547	3.0408

Table 4. Pixel-scale retrival of masses for different samples

Samples	Mean effective radius	Mean optical depth	Estimated Mass	
			in the frame	in the cloud
Sample 1	2.66746	0.65104	36,215	200,000
sample 2	2.47355	0.67467	33,170	183,000
Sample 3	2.06648	0.60572	28,325	156,000
Sample 4	2.02519	0.63987	54,812	302,000
Sample 5	1.99840	0.63788	54,938	303,000
Sample 6	2.00270	0.59291	43,191	238,000

Table 5. Frame scale retrieval for different size distributions

Retrieval parameters	Samples					
	(1) Andesite	(2) Basalt	(3) Glassy basalt	(4) Glassy rhyolite	(5) Glassy Rhyolite	(6) Volcanic dust
mean effective radius	2.6675	2.4736	2.0665	2.0252	1.9984	2.0027
mean optical depth	0.6510	0.6747	0.6057	0.6399	0.6379	0.5929
Uniform Distribution: $N(r)=1$. mean=r_e, var=0.						
mean particle radius	2.6675	2.4736	2.0665	2.0252	1.9984	2.0027
mass in a pixel	2.4009	2.1340	1.7851	2.3978	2.3677	2.6965
mass in the frame	35,671	31,705	26,521	35,624	35,177	40,061
mass in the cloud	197,000	175,000	146,000	196,000	193,824	221,000
Modified Gamma Distribution: $n(r)=(N(r_e/6)^7/6!)r^6\exp(-r_e r/6)$. mean=$7r_e/9$, var=$7r_e^2/81$.						
mean particle radius	2.0747	1.9239	1.6073	1.5752	1.5543	1.5577
mass in a pixel	2.6323	2.4763	2.1085	2.6421	2.6009	2.8647
mass in the frame	39,109	36,790	31,327	39,253	38,642	42,561
mass in the cloud	215,000	203,000	173,000	216,000	213,000	235,000
Lognormal Distribution: $n(r)=[1/(2\pi)^{1/2}\sigma r]\exp\{(\ln r-\mu)^2/2\sigma^2\}$. mean=$e^{-2\sigma^2}r_e$, var=$e^{2\mu+\sigma^2}(e^{\sigma^2}-1)$.						
mean particle radius	0.8922	0.8274	0.6912	0.6774	0.6684	0.6698
mass in a pixel	3.4864	3.4387	2.8341	3.5151	3.4631	3.5582
mass in the frame	51,798	51,089	42,106	52,223	51,452	52,864
mass in the cloud	285,000	281,000	232,000	288,000	283,000	291,000
The sensitive range of effective radius (μm) which can be uniquely retrial:						
minimum radius	0.8	1.0	0.9	2.0	2.0	0.6
maximum radius	4.3	3.1	2.9	3.1	3.1	3.2
maximum radius to get negative value of T4-T5	5.0	4.0	3.5	5.6	5.5	4.1

Note: In the above listed number, the unit of mass is in ton, and radius is micron. σ in lognormal is chosen 0.74, and $\mu=\ln(r_e)-2.5\sigma^2$ is the mean of mean of ln(r).

Figure Captions

Figure 1. Two-band temperature difference model at 10.8 μm and 11.9 μm. The solid lines represent different effective radius, and the dashed lines represent the change of optical depths at 10.8 μm along with particle radius.

Figure 2. Effective radius and normalized negative temperature domain areas. The normalized areas reflect the sensitivity of temperature difference model to the effective radius.

Figure 3. The AVHRR eruption cloud of August 19, 1992 Crater Peak/Spurr at 1338 GMT. The center square is the study frame, with an area of about 165 km × 110 km.

Figure 4. Simulated temperature pairs, the temperature differences (10.8 μm - 12 μm) and brightness temperature differences at 10.8 μm, as a function of effective radius and the optical depth, comparing with the observed AVHRR data. The small dots in the plot represent the observed data.

Figure 5. Frequency distribution of effective radius.

Figure 6. Contour map, for the study area, of the effective radius in pixel-scale retrieval. The numbers in the contour map are the effective radius in microns. Numbers on the axes indicate distances among the edge of 1.1 km pixels.

Figure 7. Contour map of the optical depth at 10.8 μm (band 4).

Figure 8. The comparison of models for different refractive index.

Figure 9. The two-band temperature difference model for $T_s - T_c = 10°C$. The absolute maximum temperature difference is reduced to about 3°C.

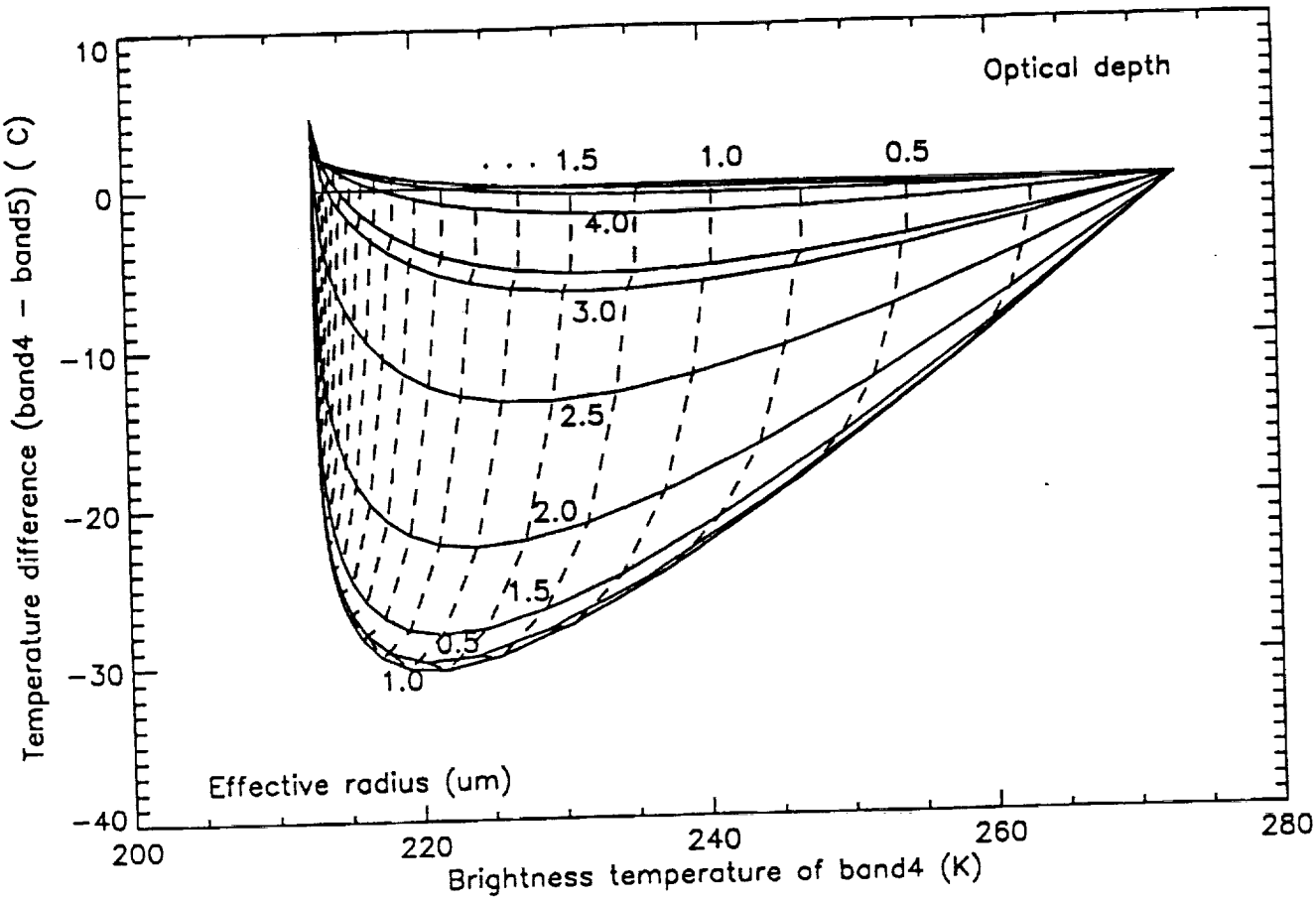
Optical depth
. . . 1.5
1.0
0.5
4.0
3.0
2.5
2.0
1.5
0.5
1.0
Effective radius (um)
Temperature difference (band4 − band5) (C)
Brightness temperature of band4 (K)
10
0
−10
−20
−30
−40
200
220
240
260
280

FIG 1

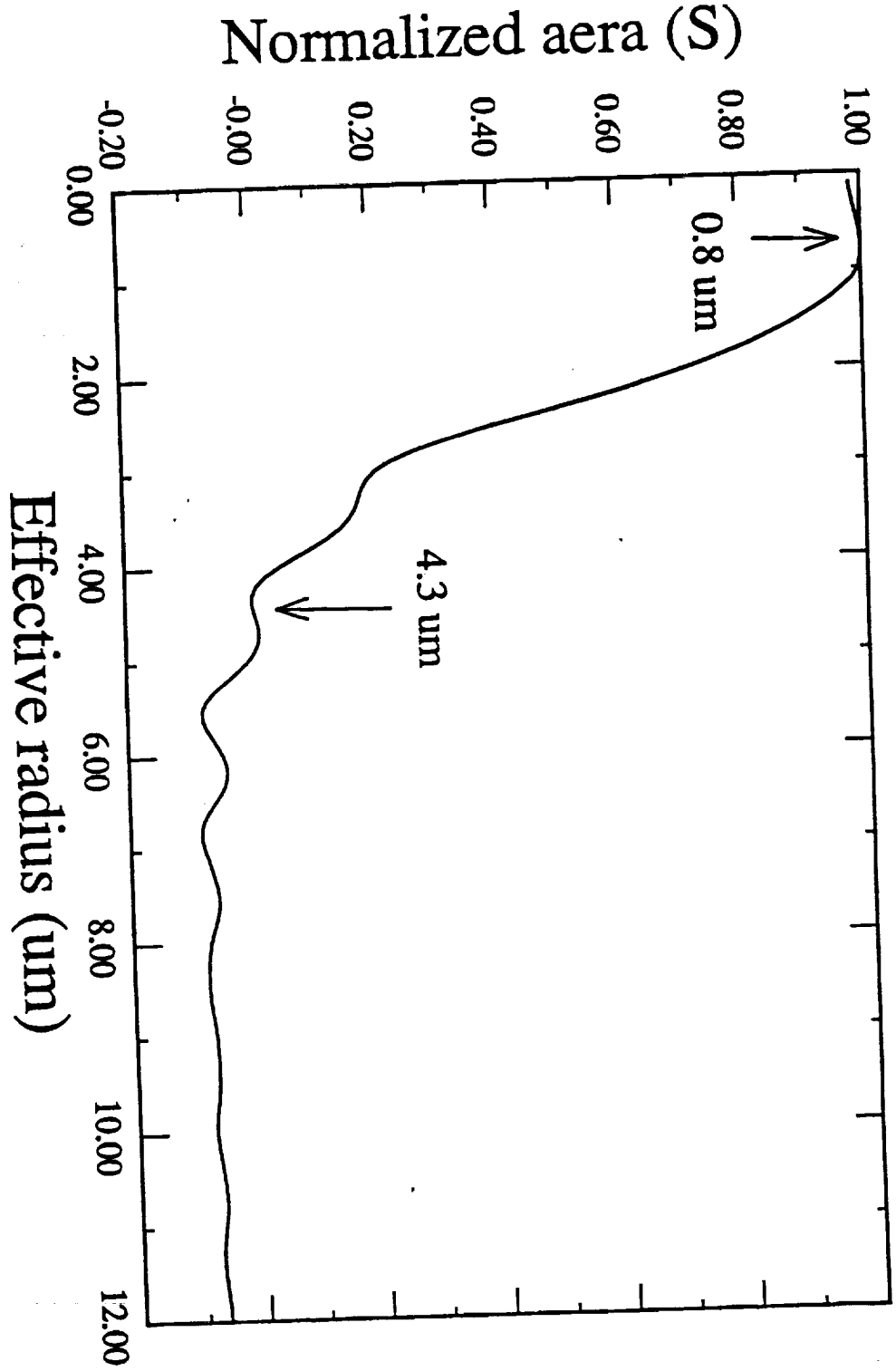
Normalized aera (S)
-0.20
-0.00
0.20
0.40
0.60
0.80
1.00
0.8 um
4.3 um
0.00
2.00
4.00
6.00
8.00
10.00
12.00
Effective radius (um)

Fig 2

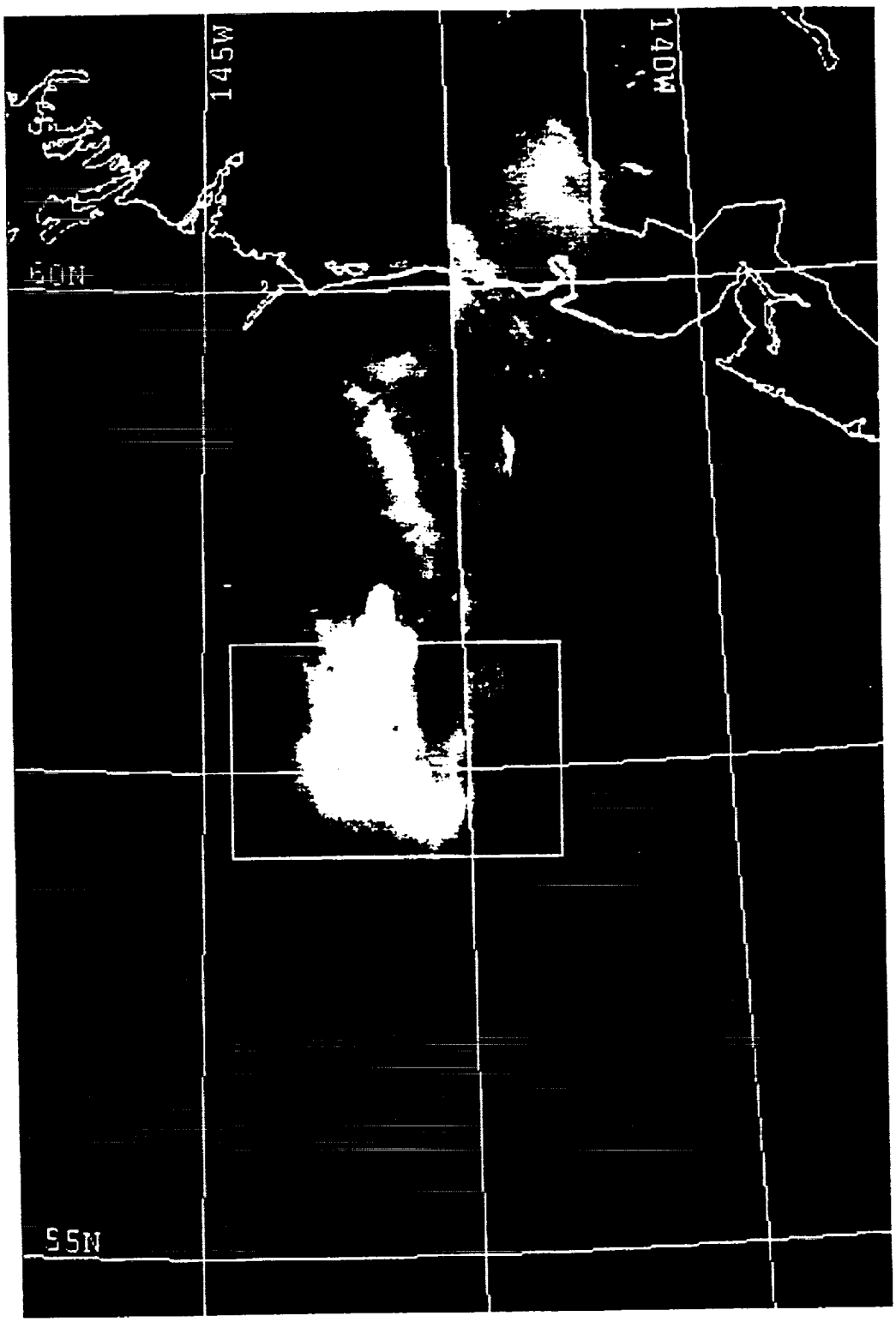

FIG 3

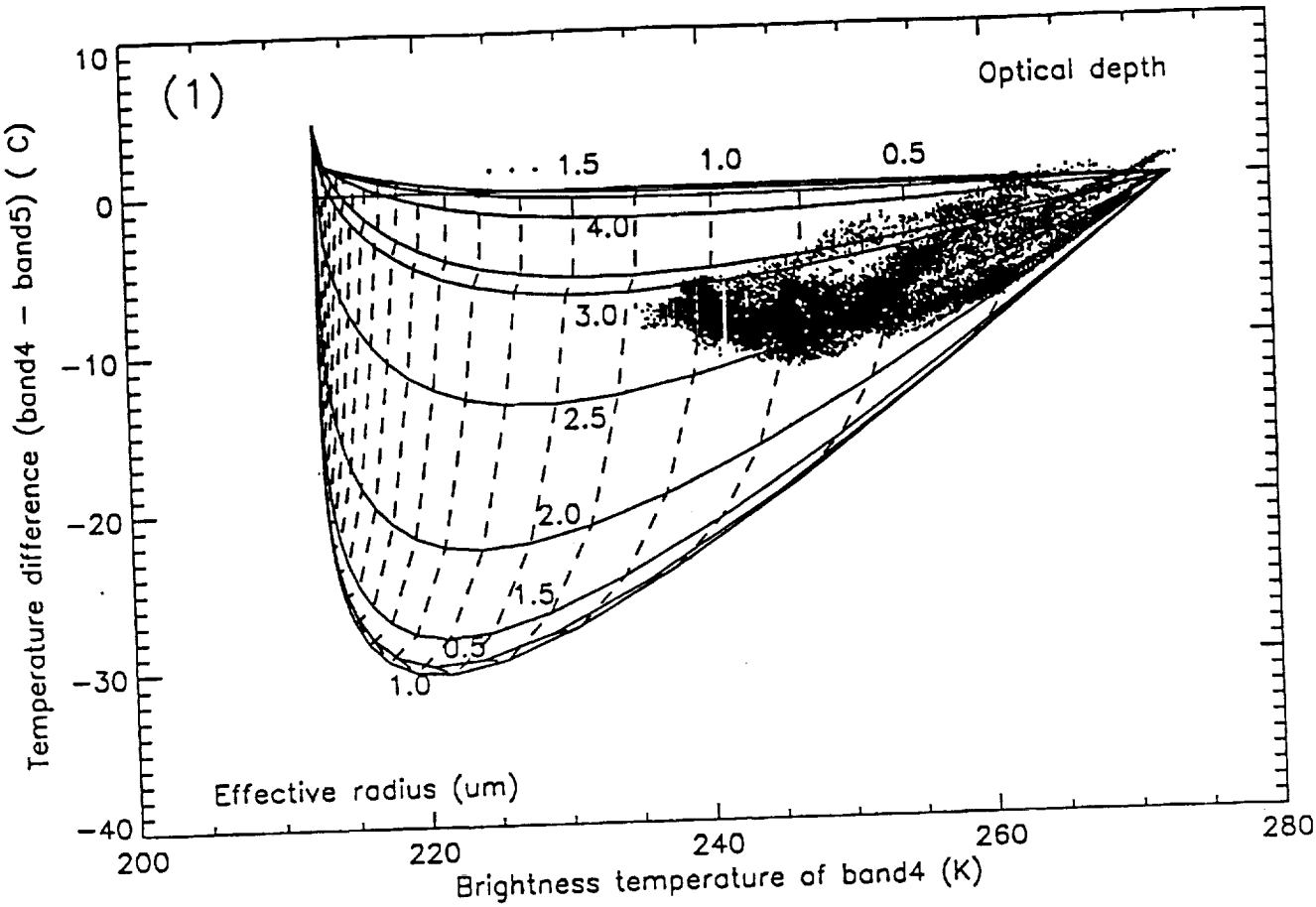
(1)
Optical depth
1.5
1.0
0.5
4.0
3.0
2.5
2.0
1.5
0.5
1.0
Effective radius (um)
Temperature difference (band4 - band5) (C)
Brightness temperature of band4 (K)
10
0
-10
-20
-30
-40
200
220
240
260
280

Fig 1

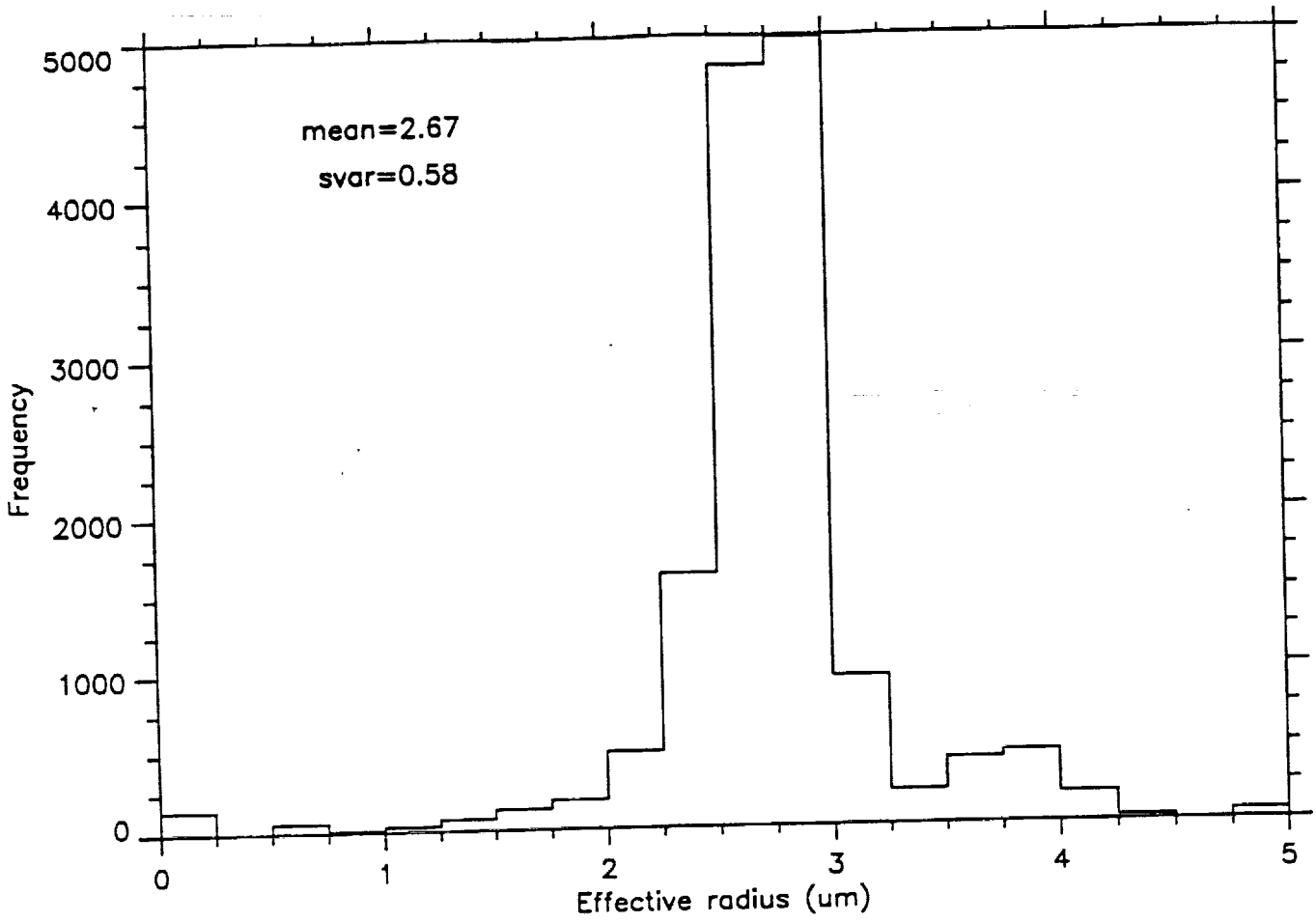
mean=2.67
svar=0.58
Frequency
Effective radius (um)
0
1000
2000
3000
4000
5000
0
1
2
3
4
5

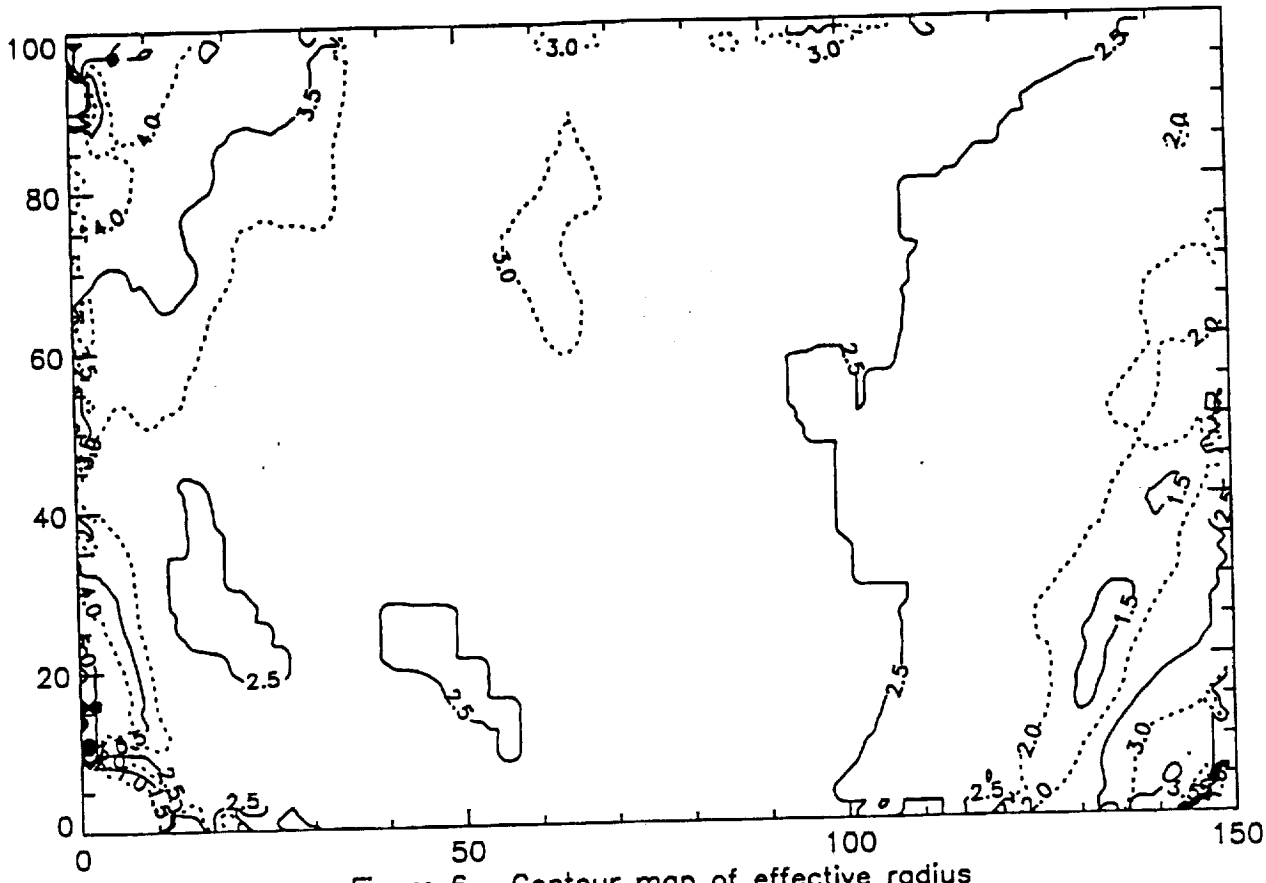

Figure 6 Contour map of effective radius

Fig 5

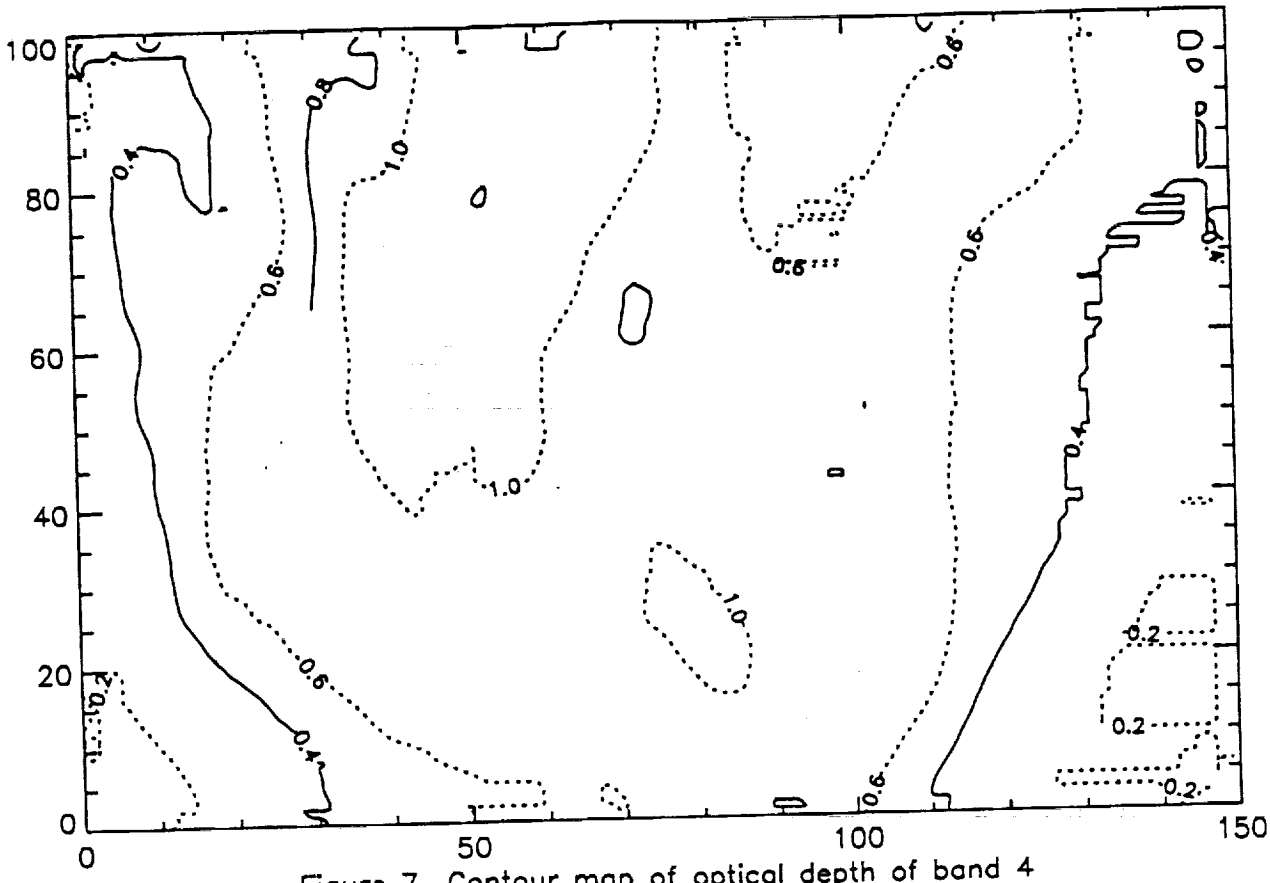

Figure 7 Contour map of optical depth of band 4

Fig 7

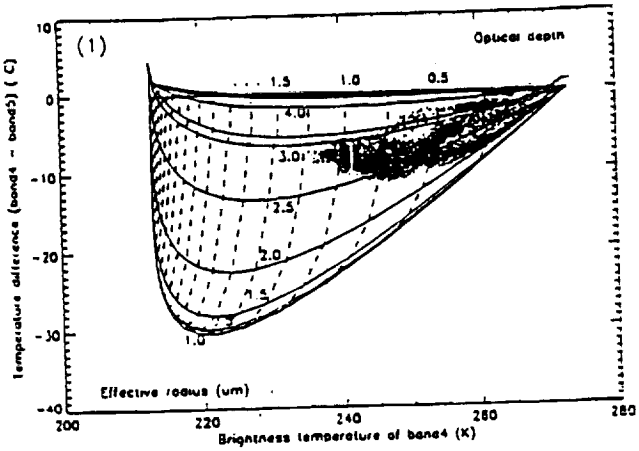
(1)
Optical depth
Temperature difference (band4 - band5) (C)
Effective radius (um)
Brightness temperature of band4 (K)

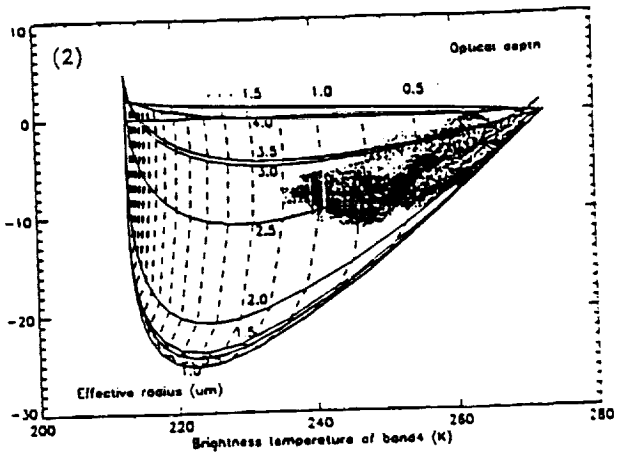
(2)
Optical depth
Effective radius (um)
Brightness temperature of band4 (K)

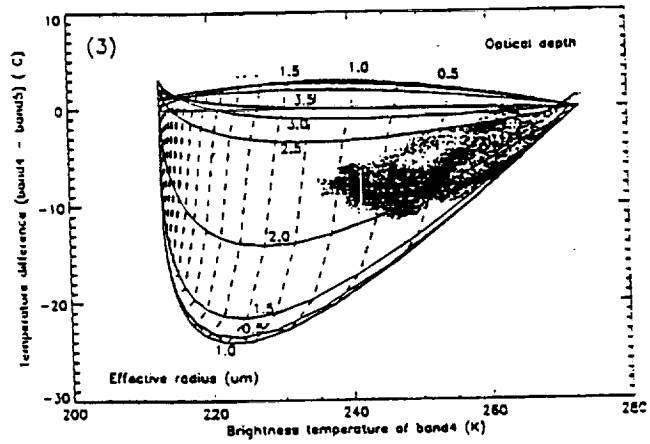
(3)
Optical depth
Temperature difference (band4 - band5) (C)
Effective radius (um)
Brightness temperature of band4 (K)

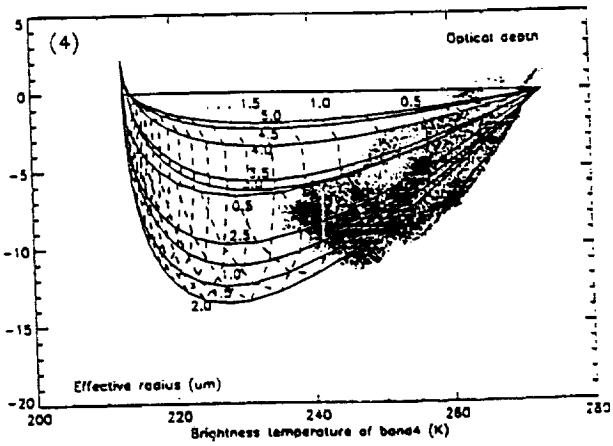
(4)
Optical depth
Effective radius (um)
Brightness temperature of band4 (K)

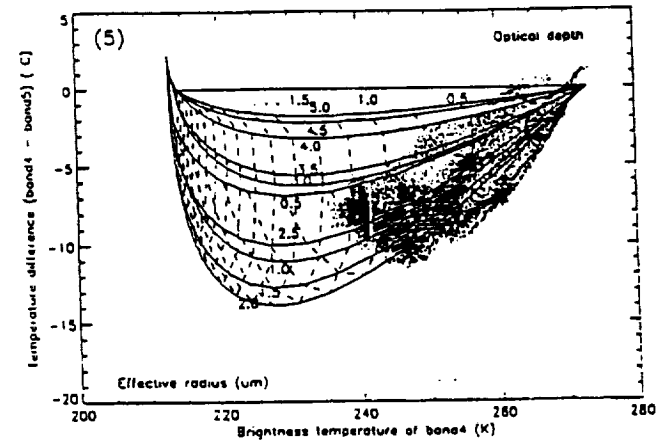
(5)
Optical depth
Temperature difference (band4 - band5) (C)
Effective radius (um)
Brightness temperature of band4 (K)

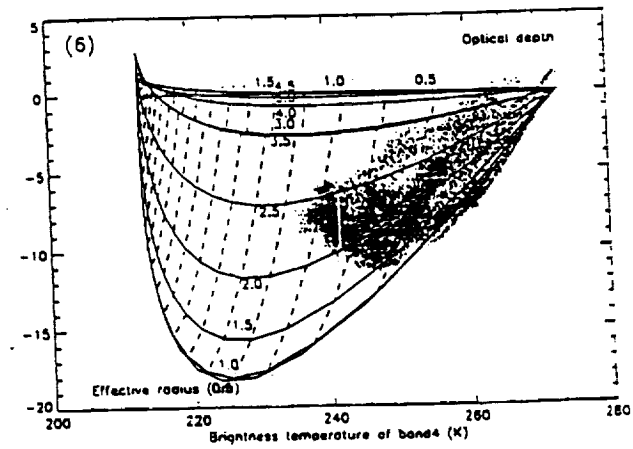
(6)
Optical depth
Effective radius (um)
Brightness temperature of band4 (K)

Fig. 2

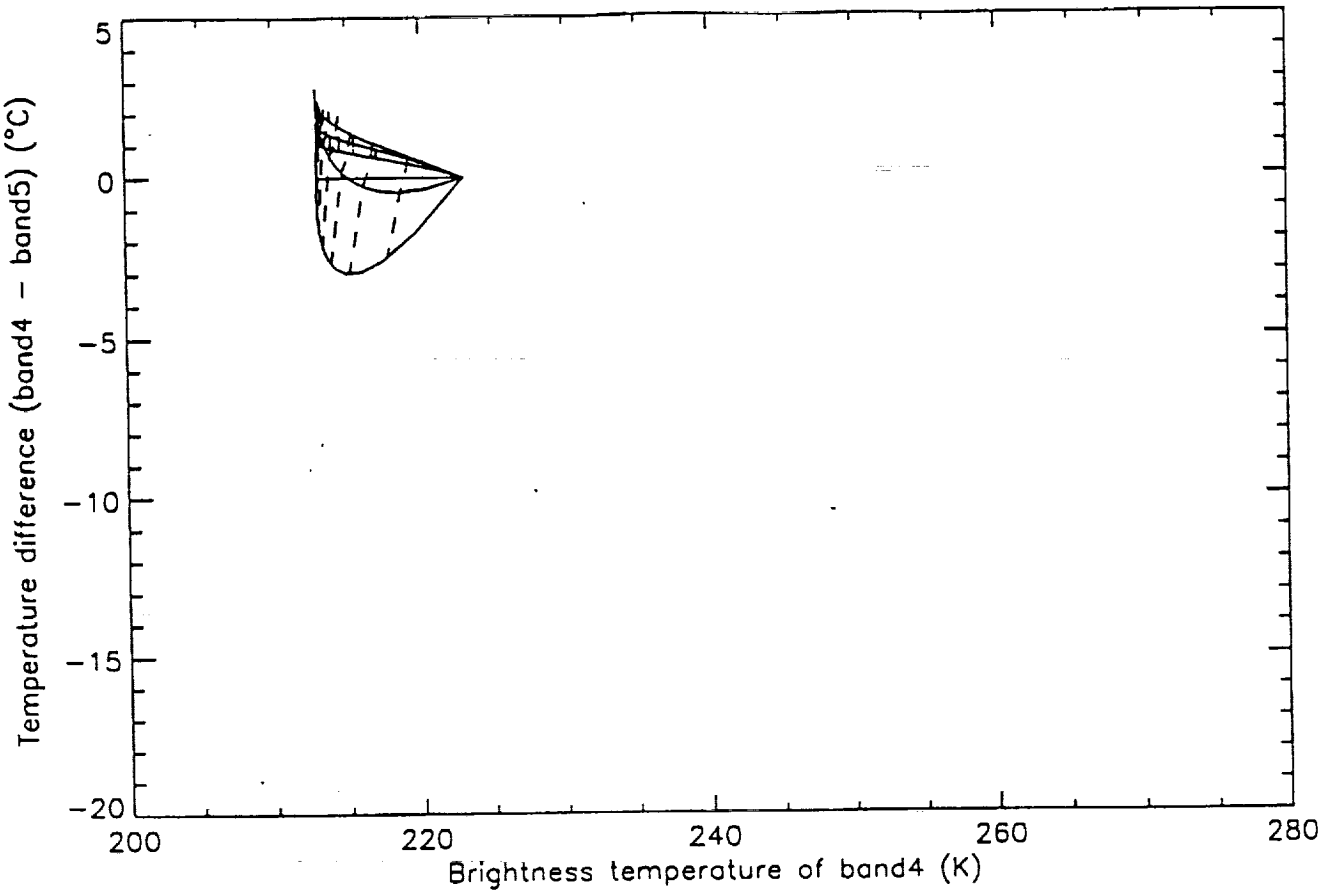
5
0
−5
−10
−15
−20
200
220
240
260
280
Temperature difference (band4 − band5) (°C)
Brightness temperature of band4 (K)

Fig 9